Photochemical & Photobiological Sciences

RSC Publishing

PAPER

Application of solution processable squaraine dyes as electron donors for organic bulk-heterojunction solar cells

Cite this: *Photochem. Photobiol. Sci.*, 2013, **12**, 1688

B. Ananda Rao,[a,b] K. Yesudas,[b] G. Siva Kumar,[a,b] K. Bhanuprakash,*[b] V. Jayathirtha Rao,*[a] G. D. Sharma*[c] and S. P. Singh[b]

Received 13th March 2013,
Accepted 15th May 2013

DOI: 10.1039/c3pp50087j

www.rsc.org/pps

New low bandgap small molecules based on a squaraine (SQ) chromophore, bis[4-(2,6-di-*tert*-butyl)vinylpyrylium]squaraine (**TBU-SQ**), bis[2,6-di-*tert*-butyl-4-(prop-1-en-2-yl)pyrylium]squaraine (**MeTBU-SQ**) and bis[4-(but-1-en-2-yl)-2,6-di-*tert*-butylpyrylium]squaraine (**EtTBU-SQ**), were synthesized and used as electron donors along with $PC_{70}BM$ for their application in solution processed organic bulk-heterojunction (OBHJ) solar cell (SC). The long wavelength of these SQ dyes are located in between 650–750 nm in thin films and the optical bandgaps are about 1.64, 1.52 and 1.48 eV, respectively. The electrochemical properties of these SQ dyes indicate that they are well suited for the fabrication of OBHJSCs as electron donors along with fullerene derivatives as electron acceptors. The OBHJ photovoltaic (PV) devices fabricated with the blend of **TBU-SQ**:$PC_{70}BM$, **MeTBU-SQ**:$PC_{70}BM$ and **EtTBU-SQ**:$PC_{70}BM$ cast from chloroform (CF) solvent exhibited a power conversion efficiency (PCE) of 1.71%, 2.15%, and 1.89%, respectively. The PCE of the OBHJSCs based on **MeTBU-SQ**:$PC_{70}BM$ blends cast from DIO–THF (DIO = 1,8-diiodooctane) additive solvent and cast from DIO–THF with subsequent thermal annealing have been further improved up to 2.73% and 3.14%, respectively. This enhancement in the PCE is attributed to the improvement in the crystalline nature of the blend and more balanced charge transport resulting from the higher hole mobility. All these results have been supported by the quantum chemical calculations.

1. Introduction

Organic solar cells (OSCs) have attracted significant attention as a clean and competitive renewable energy source due to their attractive features such as low cost, lightweight, solution processability and high mechanical flexibility.[1–6] Most of the attention has been focused on solution processed organic bulk-heterojunction solar cells (BHJSCs) based on conjugated polymers.[4,7–9] To function as electron donors for OBHJSCs, materials should exhibit broad absorption extending to the near infrared region (NIR) of the solar spectrum for light harvesting, high hole mobility for facile charge transport, energy levels well matched to those of electron acceptors for efficient charge separation and large open-circuit voltage (V_{OC}), and desirable phase separation to form continuous percolation pathways for charge transport and collection.[10] A combination of polymer design, morphology control, structural insight and device engineering has lead to PCEs reaching 6–8.3% range for conjugated polymer–fullerene blends[11–18] and recently 9.2% has been achieved.[19] For these efficient polymer SCs, the majority of reports in the literature use narrow bandgap conjugated polymers (as donor phase) in combination with a fullerene derivative (acceptor phase). However, the statistical nature of polymerization reactions lead to variability of molecular weight characteristics and ultimately in the device performance. More recently, OBHJSCs using solution processed small molecules as donors have attracted great attention due to numerous advantages over conjugated polymers, such as relatively simple synthesis and purification methods, mono-dispersity and well-defined structures, high V_{OC} and charge carrier mobilities and better batch-to-batch reproducibility.[20–31] The highest PCE of a solution processable OBHJSC based on a small molecule has reached 4.4%[26] for a DPP-thiophene derivative, 5.2% for DPP$(TBF_4)_2$:$PC_{60}BM$[32] and a record PCE of 6.7% for DTS$(PTTh_2)_2$:$PC_{70}BM$ (donor to acceptor ratio 7 : 3).[33] These results provide important progress for solution processed organic photovoltaics (OPV) and demonstrate that OBHJSCs fabricated from small donor molecules can compete with their polymer counterparts.

[a]*Crop Protection Chemicals Division, CSIR-Indian Institute of Chemical Technology, Hyderabad, Andhra Pradesh – 500 007, India*
[b]*Inorganic and Physical Chemistry Division, CSIR-Indian Institute of Chemical Technology, Hyderabad, Andhra Pradesh – 500 007, India.*
E-mail: bhanu2505@yahoo.co.in
[c]*R & D Center for Engineering and Science, JEC group of Colleges, Kukas, Jaipur, Rajasthan – 30310, India*

In general, strategies to improve the PCE of OBHJSCs include: (i) choosing the energy gaps of donor and acceptor to enhance solar energy coverage from blue to NIR leading to an increased short circuit current (J_{SC}), (ii) adjusting the highest occupied molecular orbital (HOMO) energy level of the donor and the lowest unoccupied molecular orbital (LUMO) of the acceptor as well as reducing recombination at the donor–acceptor interface to increase the V_{OC}, and (iii) improving the charge transport by extending the crystalline domain size in phase-separated donors and acceptors to increase the fill factor (*FF*). To obtain improved performance, efforts have focused on the design and synthesis of soluble donors with high charge carrier mobilities and absorption in the visible and NIR regions, in combination with a high interfacial energy gap at the donor–acceptor interface.

SQ dyes are notable for their exceptionally high absorption coefficients that can extend from the green to NIR.[34–39] Earlier SQ dyes were studied as active components for single-layer OPV during 1970–1980s, affording maximum PCE of ~0.02%, in dye-sensitized (DS) SCs[40–43] and hybrid SCs.[40,44] Forrest *et al.* have shown that solution-processed SQ followed by thermally evaporated C_{60} donor–acceptor SCs can have PCE of 4.6%,[36] when fabricated into a lamellar device that is subsequently annealed at 110 °C. Recently they have explored annealing of these SQ:$PC_{70}BM$ (1 : 6) blends in solvent vapor to create continuous crystalline pathways for hole conduction through SQ environment and achieved PCE of 5.2%.[45]

In this communication, we report the synthesis and use of SQ dyes bis[4-(2,6-di-*tert*-butyl)vinylpyrylium]squaraine (**TBU-SQ**), bis[2,6-di-*tert*-butyl-4-(prop-1-en-2-yl)pyrylium]squaraine (**MeTBU-SQ**) and bis[4-(but-1-en-2-yl)-2,6-di-*tert*-butylpyrylium]-squaraine (**EtTBU-SQ**) as effective, long-wavelength electron donors and $PC_{70}BM$ as electron acceptor in OBHJSCs and showed PCE of 1.71, 2.15 and 1.89%, respectively. The higher values of PCE for the OBHJSCs based on **MeTBU-SQ** and **EtTBU-SQ** are attributed to the higher values of both J_{SC} and V_{OC}. The OBHJSCs processed from **MeTBU-SQ**:$PC_{70}BM$ blend cast from additive DIO–THF solvent and cast from additive DIO–THF then thermally annealed showed PCE of 2.73% and 3.14%, respectively. The increase in the PCE has been attributed to the improvement of the crystalline nature of the blend, leading to the balanced charge transport due to the increase in hole mobility.

2. Experimental details

2.1. Measurements and instruments

Analytical grade reagents were used without further purification. ^{1}H NMR spectra were recorded on a Gemini (200 MHz), Bruker Avance (300 MHz), Varian (400 MHz and 500 MHz) spectrometers in $CDCl_3$ and ^{13}C NMR spectra on a Bruker Avance (75 MHz) spectrometer, both with TMS as internal standard. Mass spectra were obtained by using an electrospray ionization ion trap mass spectrometer (ESI-MS) (Thermofinnigan, Sanzox, CA, USA). UV-Visible absorption spectra were measured on a Jasco V-550 spectrophotometer and Perkin Elmer, Lambda-750, UV-Visible spectrometer. The thermal properties were determined by using thermogravimetric analysis (TGA) using a TGA–SDTA 851^e (METTLER TOLEDO) in the temperature range of 30–510 °C in N_2 atmosphere by heating at a rate of 10 °C min^{-1}. Elemental analyses were recorded on an Elementar Vario micro cube. Cyclic voltammetry studies were performed in DCM with 0.1 M $TBAPF_6$ as supporting electrolyte with glassy carbon as working electrode, a platinum wire as counter electrode and saturated calomel electrode as reference electrode for evaluating the electrochemical properties. The crystallinity of the films was studied using the X-ray diffraction (XRD) technique (Panalytical make, USA), having CuK_α, as radiation source of wavelength λ = 15 405 Å with the films coated on quartz substrates.

OBHJSC devices were fabricated through the solution processing technique. Patterned indium tin oxide (ITO) coated glass substrates were subsequently cleaned with detergent, deionized water, acetone and isopropanol and then dried at room temperature for 30 min in ambient conditions. A thin layer of poly(3,4-ethylene dioxythiophene):poly(styrenesulfonate) (PEDOT:PSS) (80 nm) was spin coated onto the cleaned ITO glass substrate and subsequently dried at 80 °C for 20 min. The solution of blend SQ dyes:$PC_{70}BM$ (1 : 1, 1 : 2, 1 : 3 and 1 : 4 w/w) were prepared in concentration of 5 mg mL^{-1} using THF as solvent and stirred for 2 h for the mixed solvent, 0.6% by volume of DIO was added to the blend solution in THF and then stirred for 2 h. The photoactive layer of blend was deposited from the solution of blend in THF and mixed solvent by a spin coating technique. The thickness of the active layers was in the range of 80–90 nm. The organic films were dried in vacuum at room temperature. An aluminum (Al) cathode (90 nm) was then thermally evaporated under high vacuum (10^{-5} Torr) through a shadow mask defining an active area of 0.05 cm^2. The pre-thermal annealing of the active layer was carried out at 110 °C for 2 min on a hot plate before deposition of the Al electrode.

Current–voltage (*J–V*) characteristics of the devices were measured using a computer-controlled Keithley 238 source meter in dark and under an illumination intensity of 100 mW cm^{-2}, under ambient conditions. A halogen lamp source (100 W) coupled with AM 1.5 solar spectrum filters was used as light source and optical power at the surface of the device was 100 mW cm^{-2}. Hole or electron only devices were fabricated using the architectures ITO/PEDOT:PSS/SQ:$PC_{70}BM$/Au for holes and Al/SQ:$PC_{70}BM$/Al for electrons. Mobilities were extracted by fitting the *J–V* curves using the Mott–Gurney relationship,[46] *i.e.* space charge limited current (SCLC).

$$J_{SCLC} = (9/8)\varepsilon_o\varepsilon_r\mu(V^2/L^3)$$

where J_{SCLC} is the current density in the SCLC regime, L is the film thickness of active layer, μ is the hole mobility, ε_r is the relative dielectric constant of the organic donor layer (assuming), ε_o is the permittivity of free space and V is the applied voltage. The incident photon to current conversion efficiency

(IPCE) of the devices was measured by illuminating the device through the light source coupled with monochromator, and the resulting photocurrent was measured using a Keithley electrometer under short circuit conditions. The value of the IPCE value at each wavelength (λ) was estimated using following expression

$$\mathrm{IPCE}(\lambda) = 1240 J_{SC}/P_{in}\lambda$$

where J_{SC} is the photocurrent under short circuit condition and P_{in} is incident illumination intensity.

2.2. Synthesis and characterization

2.2.1. Procedure for the synthesis of 4-alkyl (methyl/ethyl/propyl)-2,6-di-*tert*-butyl pyrylium perchlorates.[47] (PY1–PY3, Scheme 1a). A dry round-bottomed flask charged with 28.35 mL (30.6 g, 0.3 mol) of acetic anhydride was cooled to −10 °C under nitrogen atmosphere. 6.22 mL (10 g, 0.1 mol) of pre-cooled perchloric acid (70%)was added drop-wise to acetic anhydride. The solution was added to an ice-cooled and well-stirred mixture of pinacolone (10.0 g, 0.1 mol) and triethylorthoformate (44.5 g, 0.3 mol) and the reaction mixture was stirred at 0 °C for 30 min. The reaction mixture was poured into diethyl ether (~300 mL), a white solid precipitated out and was filtered out through a Buchner funnel. The collected solid was purified by crystallization from ethanol. The salt 2,6-di-*tert*-butylpyrylium perchlorate was obtained in 60% yield.

2,6-di-*tert*-Butyl pyrylium perchlorate: mp: 229–231 °C; ^{1}H NMR ($CDCl_3$) δ: 9.08 (t, 1H, J = 8.3 Hz), 8.20 (d, 2H, J = 8.3 Hz), 1.56 (s, 18H); MS (ESI +ve): m/z 193 $(M)^+$.

A two phase solution (120 mL dichloromethane and 240 mL distilled water) of acetic acid (7.5 mL, 0.125 mol) for **PY1**, propionic acid (9.3 mL, 0.125 mol) for **PY2** or butyric acid (11.5 mL, 0.125 mol) for **PY3**, 2,6-di-*tert*-butylpyrylium perchlorate, (7.3 g, 0.025 mol), $K_2S_2O_8$(10.125 g, 0.0375 mol) and $AgNO_3$ (0.211 g, 0.00125 mol) was heated for 4 h at 40 °C. The reaction mixture was cooled to room temperature and extracted with dichloromethane, washed with 5% $HClO_4$ (~100 mL) once and with water twice (2 × 150 mL). After being dried over $CaCl_2$, the solution was concentrated to about 5 mL and added to 100 mL diethyl ether and kept in a refrigerator for overnight. A solid precipitated out and was filtered through a Buchner funnel. The precipitate was crystallized from ethanol–water (15 mL–3 drops) to give fine needles. Yields were 60%, 54% and 50% for **PY1**, **PY2** and **PY3** respectively.

PY1: mp: 230–232 °C; ^{1}H NMR ($CDCl_3$) δ: 8.08 (s, 2H), 2.83 (s, 3H), 1.52 (s, 18H); ^{13}C NMR ($CDCl_3$) δ: 185.2, 176.5, 120.3, 38.7, 27.9, 24.4; MS (ESI +ve): m/z 207 $(M)^+$; IR (KBr): 3055, 2981, 1633, 1538, 1272, 1145, 1032, 636; HRMS (m/z): calculated for $C_{14}H_{23}O$, 207.1748, found, 207.1744.

PY2: mp: 151–153 °C; ^{1}H NMR ($CDCl_3$) δ: 7.94 (s, 2H), 3.09 (q, 2H, J = 7.3 Hz), 1.52, (s, 18H), 1.40 (t, 3H, J = 7.3 Hz); MS (ESI +ve): m/z 221 $(M)^+$.

PY3: mp: 83–85 °C; ^{1}H NMR ($CDCl_3$) δ: 7.75 (s, 2H), 3.03–3.06 (q, 2H, J = 7.8 Hz), 1.80–1.85 (m, 2H), 1.51, (s, 18H), 1.03 (t, 3H, J = 7.8 Hz); MS (ESI +ve): m/z 235 $(M)^+$.

2.2.2. Procedure for the synthesis of SQ dyes. The synthesis of SQ dyes is shown in Scheme 1b.[47–49] A mixture of 786 mg (3.8 mmol) of **PY1**, 839 mg (3.8 mmol) of **PY2** or 893 mg (3.8 mmol) of **PY3**, squaric acid (216 mg, 1.9 mmol) and quinolone (490 mg, 3.8 mmol) in 40 mL of *n*-butanol, 160 mL of absolute toluene was refluxed for 3–5 h with azeotropic removal of water and monitoring the reaction with UV-Visible spectrophotometer up to complete disappearance of pyrylium salt and squaric acid. After cooling to room temperature, solvent was removed by rotary evaporation, and then added 100 mL of diethyl ether. The precipitate formed was filtered out through a Buchner funnel and washed with diethyl ether (3 × 100 mL) to remove excess quinoline. The solid was purified by column chromatography (2 : 98 $CHCl_3$–hexane) to afford pure products. All the SQ dyes showed high thermal stabilities with decomposition temperatures (T_d) started from 248 °C (with a wt loss of less than 5%).

TBU-SQ: isolated yield: 51% (475 mg); mp: 240–242 °C; ^{1}H-NMR ($CDCl_3$) δ: 8.63 (s, 2H), 6.18 (s, 2H), 5.80 (s, 2H), 1.34 (s, 18H), 1.28 (s, 18H); ^{13}C-NMR ($CDCl_3$) δ; 171.5, 170.6, 149.6, 109.2, 108.6, 104.4, 36.7, 36.4, 28.0, 27.9; MS (ESI): m/z 491 $(M + H)^+$; IR (KBr): 3416, 3055, 2965, 2863, 1640, 1604, 1566, 1487, 1345, 1271, 1208, 1107, 1079, 929; elemental analysis

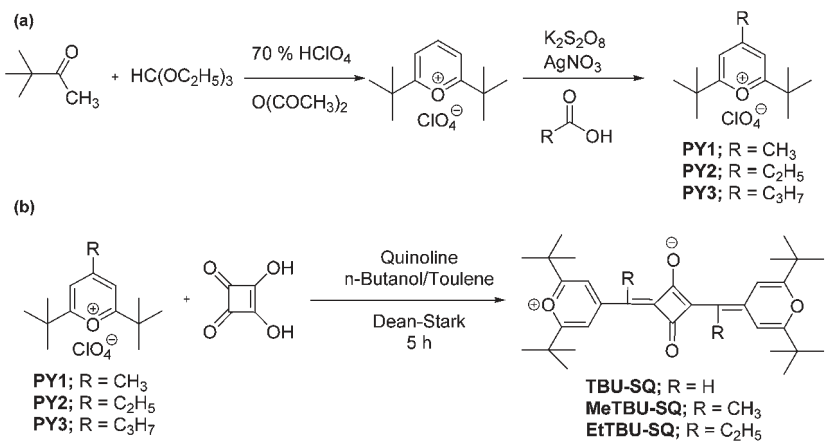

Scheme 1 Synthesis of (a) pyrylium salts (**PY1–PY3**) and (b) SQ dyes.

calcd (%) for $C_{32}H_{42}O_4$: C 78.33, H 8.63; found: C 77.95, H 8.80. HRMS (*m*/*z*): [M + H] calculated for $C_{32}H_{43}O_4$, 491.3161, found, 491.3143.

MeTBU-SQ: isolated yield: 54% (606 mg); mp: 270–273 °C; ^{1}H-NMR($CDCl_3$) δ: 8.86 (s, 2H), 6.26 (s, 2H), 2.29 (s, 6H), 1.33 (s, 18H), 1.30 (s, 18H); ^{13}C-NMR ($CDCl_3$) δ; 179.2, 171.0, 167.7, 146.3, 110.7, 104.3, 36.6, 28.1, 28.0, 13.5; MS (ESI): *m*/*z* 519 $(M + H)^+$; IR (KBr): 3421, 2964, 1640, 1591, 1470, 1413, 1358, 1298, 1210, 1153, 1085, 928; elemental analysis calcd (%) for $C_{34}H_{46}O_4$: C 78.72, H 8.94; found: C 78.69, H 8.76. HRMS (*m*/*z*): [M + H] calculated for $C_{34}H_{47}O_4$, 519.3474, found, 519.3485.

EtTBU-SQ: isolated yield: 41% (426 mg); mp: 220–223 °C; ^{1}H-NMR($CDCl_3$) δ: 8.76 (s, 2H), 6.86 (s, 2H), 6.32 (s, 2H), 2.83–2.90 (q, 4H, J = 7.5 Hz), 1.31 (s, 36H), 1.06 (t, 3H, J = 7.5 Hz); MS (ESI): *m*/*z* 547 $(M + H)^+$; IR (KBr): 3421, 2960, 2924, 2863, 1734, 1634, 1585, 1457, 1413, 1361, 1313, 1270, 1240, 1210, 1147, 1088, 1054, 1028, 922; elemental analysis calcd (%) for $C_{36}H_{50}O_4$: C 79.08, H 9.22; found: C 79.10, H 9.30. HRMS (*m*/*z*): [M + H] calculated for $C_{36}H_{51}O_4$, 547.3787, found, 547.3780.

2.3. Quantum chemical calculations

Quantum chemical calculations have been performed to give a deeper insight into the electronic structure, absorption properties and PV performance using the density functional theory (DFT) implemented in Gaussian 09 program.[50] The geometries of all the SQ dyes were optimized at the hybrid DFT-B3LYP level with $C_{2h}/C_{2h}/C_2$ symmetry constraint for **TBU-SQ**/**MeTBU-SQ**/**EtTBU-SQ** by replacing the computationally bulkier *tert*-butyl group with a methyl group and followed by vibrational frequency analysis. The geometries optimized are found to be minima on the potential energy surface characterized by the real values for frequencies. The parent SQ showed very small geometric changes in the structural parameters by 0.001–0.004 Å in the bond lengths and 0.9° in the central SQ (C–C–C) angle with the substitution of a hydrogen atom for the methyl and ethyl groups at the vinylic position. The 30 lowest optical transition energies have been obtained by using the symmetry adapted cluster-configuration interaction (SACCI)[51–53] method at level two by considering 160 orbitals in the active space (40 occupied and 120 unoccupied). In all these calculations we employed the 6-31G(d,p) basis set.

3. Results and discussion

3.1. Optical absorption

The normalized absorption spectra of all the SQ dyes in THF are shown in Fig. 1. These SQ dyes show the characteristic strong narrow long wavelength absorption band typical of SQ compounds having an absorption peak around 720, 765 and 758 nm (1.72, 1.62 and 1.63 eV) for **TBU-SQ**, **MeTBU-SQ** and **EtTBU-SQ**, respectively. The respective redshifts of 45 and 38 nm in **MeTBU-SQ** and **EtTBU-SQ** compared to the parent

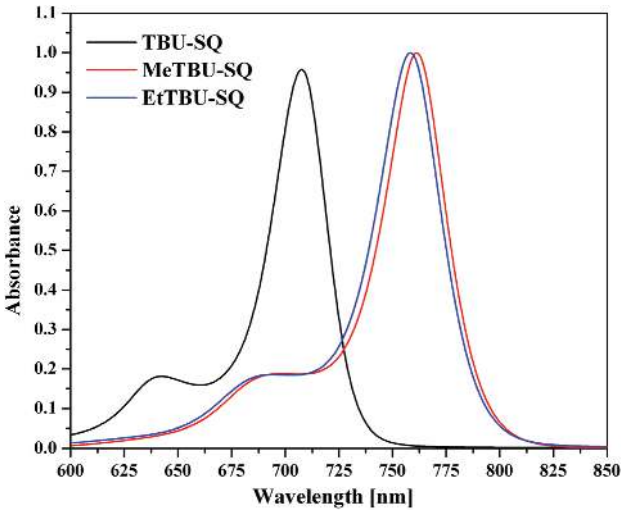

Fig. 1 Normalized absorption spectra of all the SQ dyes in THF.

TBU-SQ is attributed to the presence of charge-donating methyl and ethyl groups at the vinylic position exerting a positive inductive effect. A very small blueshift of 7 nm in **EtTBU-SQ** compared to **MeTBU-SQ** is attributed to the steric effect of the ethyl group at the vinylic position with the squaric acid ring and makes the ethyl group deviate slightly from planarity. The optical energy bandgaps estimated from the onset absorption wavelengths are 1.64, 1.52 and 1.54 eV for **TBU-SQ**, **MeTBU-SQ** and **EtTBU-SQ**, respectively, which are lower than the conjugated polymers.

The detailed analysis of these long wavelength absorptions and their nature can be made on the basis of quantum chemical calculations. The electronic absorption properties obtained using SACCI method are collected in Table 1. The calculated wavelength values for these dyes are 711, 744 and 739 nm (1.74, 1.67 and 1.68 eV) ($^1A_g \rightarrow {}^1B_u/A \rightarrow B$; $\pi \rightarrow \pi^*$) with oscillator strengths of 1.365, 1.317 and 1.267, respectively. The wavelengths are slightly under estimated by 9, 21 and 19 nm, respectively, but followed the trend with the experiment. This underestimation is probably due to the fact that the calculations have been performed in the vacuum state while the measurements have been performed in solution, which has additional intermolecular interaction effects as well as differences in the incorporation of the correlation energies in the ground and excited states at the SACCI level. As these molecules are oriented in *XY*-plane, these transitions are *X*- and *Y*-polarized as seen from the ground to first excited state transition dipole moments (Table 1), while the dominant one is *Y*-polarized (molecular long axis) with an average magnitude of ~13.3 D (94% to the total dipole moment). These transitions are described as a single particle–hole excitation and at the orbital level mainly dominated by the transition from the HOMO (a_u/a) → LUMO (b_g/b) with ~94% of the CI-coefficient. These transitions are accompanied by a less prominent transition from HOMO − 1 (b_g/b) → LUMO + 1 (a_u/a) (~11%), which can be seen from the one-electron density profiles in

Table 1 Experimental and calculated ground-to-first excited state absorption wavelengths (λ^{expt} and λ^{cal} in nm), resolved and total ground-to-excited state transition dipole moments (μ^{x}_{ge}, μ^{y}_{ge}, μ^{T}_{ge} in D)[a], oscillator strength (f) and the CI-singles wave function (CI coefficient >0.05) of SQ dyes obtained at SACCI/6-31G(d,p) level

SQ dye	λ^{expt}	λ^{cal}	μ^{x}_{ge}	μ^{y}_{ge}	μ^{T}_{ge}	f	CI-singles wavefunction
TBU-SQ	720	711	5.4	13.2	14.3	1.365	HOMO → LUMO (0.935) + HOMO − 1 → LUMO + 1 (0.122)
MeTBU-SQ	765	744	5.8	−13.1	14.3	1.317	HOMO → LUMO (−0.933) + HOMO − 1 → LUMO + 1 (−0.114)
EtTBU-SQ	758	739	−2.3	−13.7	13.9	1.267	HOMO → LUMO (−0.936) + HOMO − 1 → LUMO + 1 (−0.093)

[a] Due to the approximate symmetry, $\mu^{z}_{ge} = 0$.

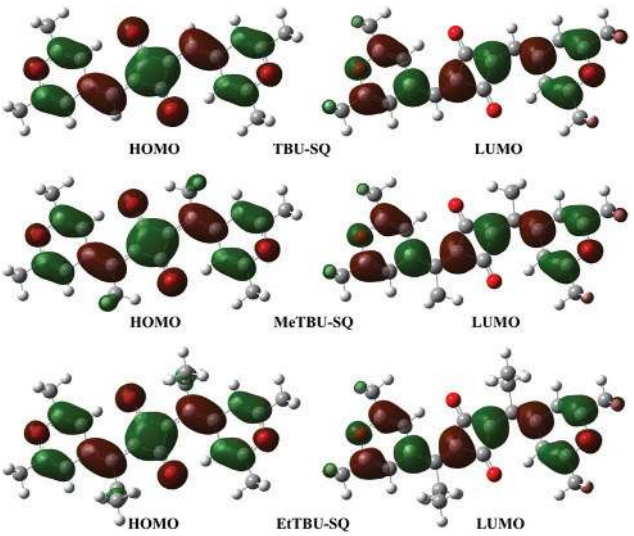

Fig. 2 Frontier one-electron molecular orbitals of all the SQ dyes obtained at B3LYP/6-31G(d,p).

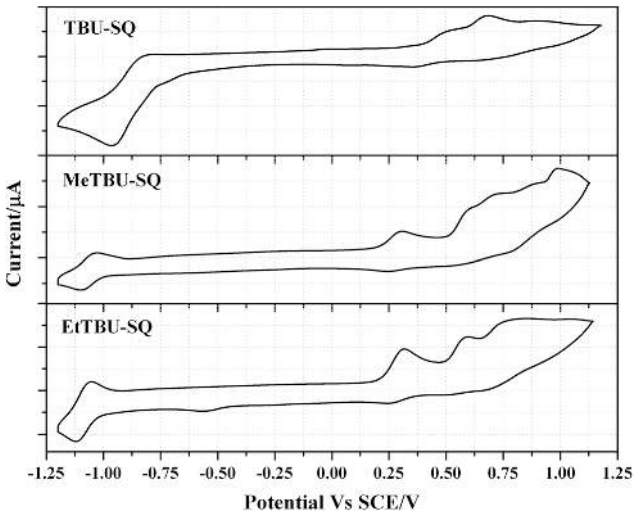

Fig. 3 Cyclic voltammograms of all the SQ dyes in DCM.

Fig. 2. The redshift of ~28 nm in the case of **MeTBU-SQ** and **EtTBU-SQ** is due to the contribution of electron density to the central ring from the methyl and ethyl groups (positive inductive effect) present at the vinylic position. Moreover, the rearrangement of electron densities (Fig. 2) and the charge-transfer analyses in the ground and first excited states suggest that these transitions are not due to intramolecular charge transfer, but are a kind of charge rearrangement occurring in the central SQ ring, as reported earlier.[54]

We have also recorded optical absorption spectra of all the SQ dyes in thin-film form and found that the absorption of these SQ dyes in thin-film form is broad and also covers 600–800 nm regions, where the solar photon flux is maximal. In thin-film form, the maximum absorption bands of these SQ dyes is red shifted and broadened compared to those in solution, which is beneficial for better light harvesting of the solar spectrum.

3.2. Electrochemical properties

The electrochemical properties of these SQ dyes were investigated to determine the HOMO and LUMO energies using cyclic voltammetry, shown in Fig. 3, and the values are compiled in Table 2. The HOMO and LUMO energy levels can be deduced from the oxidation (E^{onset}_{ox}) and reduction (E^{onset}_{red}) onset potentials respectively, with the assumption that the energy of ferrocene (Fc) is 4.945 eV, below the vacuum level.[55,56] It can be seen from the table that the HOMO of the SQ dyes is almost the same but the LUMO is sensitive to the methyl and ethyl groups attached to the carbon atom at the vinylic position. The V_{OC} of BHJSCs is correlated with the difference between the HOMO of donor and the LUMO of acceptor. In order to increase the V_{OC}, this difference should be maximized. In addition, the LUMO of the donor should be at least 0.2–0.3 eV higher than the acceptor to ensure efficient electron transfer from donor to acceptor. As shown in Table 2, the HOMOs of all these dyes are quite low compared to the LUMO of $PC_{70}BM$ and their LUMOs are more than 0.3 eV higher than that of $PC_{70}BM$. Therefore, all these SQ dyes can

Table 2 Onset of reduction and oxidation potentials (E^{onset}_{red}, E^{onset}_{ox}, volts), HOMO, LUMO energies and HLG (eV) of SQ dyes

SQ dye[a]	E^{onset}_{red}[b]	E^{onset}_{ox}[b]	HOMO[c]	LUMO[c]	HLG
TBU-SQ	−0.74	0.38	−4.78	−3.66	1.12
MeTBU-SQ	−1.12	0.24	−4.64	−3.28	1.36
EtTBU-SQ	−1.12	0.23	−4.63	−3.28	1.35
$PC_{70}BM$			−5.87	−3.91	

[a] Measured in dichloromethane. [b] Determined by cyclic voltammetry *vs.* SCE. [c] *vs.* vacuum.

be utilized as electron donor materials in the fabrication of BHJSCs.

To have a deep understanding, the fundamental electronic properties of SQ dyes and $PC_{70}BM$ are calculated using DFT and presented in Table 3. As seen from the table, the calculated energy values for HOMO and LUMO are different from experiment by average values of 0.40 and 0.96 eV, respectively. This is due to a smaller amount of exact exchange in the hybrid functional. Consequently this error is carried forward to the energy gaps (HLG), vertical and adiabatic ionization potentials and electron affinity but followed the trend with the experiment. The parent SQ is more sensitive to the substitution of the hydrogen atom with methyl and ethyl groups, as seen from the destabilization of both the HOMO and the LUMO by ~0.1 and ~0.02 eV, respectively. This observation is in good agreement with the experimental values (Table 2) for the shift of HOMO and LUMO levels with respect to **TBU-SQ** (0.13 and 0.38 eV). Shifting the LUMOs by 1.0 eV matches with experimental destabilization energy of LUMO. The adiabatic ionization potential (IP_a) values are respectively 5.52, 5.37 and 5.37 eV (Table 3) and follow the order: **MeTBU-SQ** ≅ **EtTBU-SQ** < **TBU-SQ**. The relatively small IP_a value of **MeTBU-SQ** shows that this dye undergoes oxidation relatively much faster than the other two dyes and can be a good donor in conjunction with the $PC_{70}BM$ acceptor and expected to have improved cell efficiency compared to the **TBU-SQ** and **EtTBU-SQ**. The substitution of the ethyl group has no significant impact on the electronic properties, as is evident from the similar HOMO, LUMO and IP_a values (Table 4) to that of the methyl-substituted one. The small vibronic relaxation of 0.14 eV in the IP_a compared to IP_v suggests that these dyes have less potential loss and can inject the electron into the acceptor LUMO level effectively. The calculated V_{OC} values are 1.28, 1.17 and 1.19 V, respectively, suggest that the device fabricated from **MeTBU-SQ** will have large efficiency. These values are largely deviated due to the large shift in the calculated LUMO level of the $PC_{70}BM$ by 0.87 eV but the trend for V_{OC} is retained.

Table 3 Calculated HOMO and LUMO energies, HLG, vertical and adiabatic ionization potential (IP_v and IP_a) of SQ dyes and adiabatic electron affinity (EA_a) of $PC_{70}BM$ at B3LYP/6-31G(d,p) level. All the quantities are in eV

SQ dye	HOMO	LUMO	HLG	IP_v	IP_a	EA_a
TBU-SQ	−4.33	−2.44	1.89	5.65	5.52	
MeTBU-SQ	−4.21	−2.40	1.81	5.50	5.37	
EtTBU-SQ	−4.24	−2.42	1.82	5.50	5.37	
$PC_{70}BM$	−5.55	−3.04	2.50			−2.01

Table 4 Photovoltaic parameters of OBHJSCs based on different SQ dyes as electron donors and $PC_{70}BM$ as electron acceptors cast under different conditions

SQ dye	J_{SC} (mA cm^{-2})	V_{OC} (V)	*FF*	PCE (%)
TBU-SQ[a]	6.25	0.76	0.36	1.71
MeTBU-SQ[a]	7.2	0.68	0.44	2.15
EtTBU-SQ[a]	6.82	0.66	0.42	1.89
MeTBU-SQ[b]	8.62	0.66	0.48	2.73
MeTBU-SQ[c]	9.8	0.64	0.50	3.14

[a] Blend cast from THF. [b] Blend cast from DIO–THF. [c] Blend cast from DIO–THF (thermally annealed).

3.3. Photovoltaic properties of TBU-SQ:$PC_{70}BM$ blend films

For an efficient OBHJSC, there should be a balance between the absorbance and the charge-transporting network of the active layer used in these devices. The ratio of donor and acceptor ($PC_{70}BM$) materials used for the BHJ active layer is also a crucial factor for the PCE of SC. Too low content of $PC_{70}BM$ will limit the electron transporting ability, while too high content of $PC_{70}BM$ will decrease the absorbance and hole transporting ability of the active layer. We have fabricated the BHJSCs with a different ratio (1 : 1, 1 : 2, 1 : 3 and 1 : 4 w/w) and found that the optimized ratio is 1 : 3. $PC_{70}BM$ was selected as the acceptor due to its stronger light absorption in the visible region compared to PCBM.[57] The optimum thickness of these BHJ films obtained under these conditions was approximately about 90 nm. Fig. 4 shows the UV-visible absorption spectra of **MeTBU-SQ**:$PC_{70}BM$ films. Similar absorption spectra have also been observed for other blends. The optical absorption spectra of the blend show a combination of the individual components, *i.e.* the absorption in lower wavelength region corresponds to $PC_{70}BM$ and higher wavelength region corresponds to SQ dye. The blend shows a broad absorption band from 350 nm to 800 nm. The optical absorption of the **MeTBU-SQ**:$PC_{70}BM$ blend cast from DIO–THF mixed solvent is also shown in Fig. 4. As shown in Fig. 4, the absorption band of **MeTBU-SQ** in the **MeTBU-SQ**:$PC_{70}BM$ BHJ film deposited from DIO–THF solvent was slightly redshifted compared to the cast from THF, and this peak is further broadened and redshifted when the blend is thermally annealed. The redshift and broadening of the absorption band indicate the higher degree of the crystallinity due to the enhanced interchain π–π stacking as reported for conjugated polymers.[58–66] The redshift in the absorption band corresponding to the SQ dye is also related to the J-aggregation.[67]

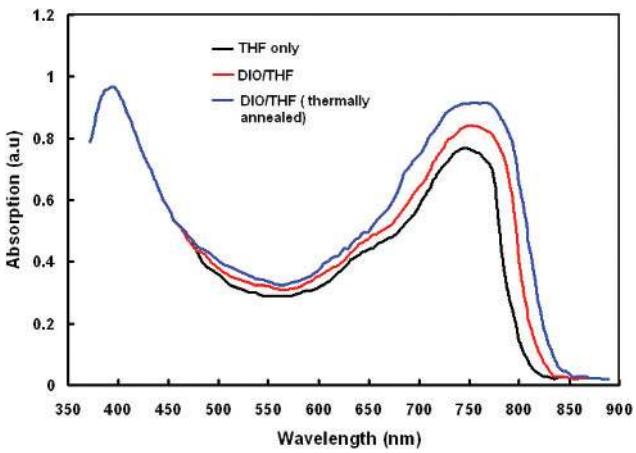

Fig. 4 Optical absorption spectra of **MeTBU-SQ**:$PC_{70}BM$ (1 : 3 w/w) cast under different conditions.

To demonstrate potential applications of these SQ dyes as electron donors and $PC_{70}BM$ as acceptor in OBHJSCs, we have varied the donor-to-acceptor ratio for the active blend cast from CF solvent and investigated the PV properties and found the V_{OC} is insensitive to the donor–acceptor weight ratio, while the J_{SC}, *FF* and PCE of the devices are strongly dependent on the donor-to-acceptor ratio in the active blend layers. The donor–acceptor weight ratio of 1 : 3 gave the best performance and the current–voltage (*J–V*) characteristics of a ITO/PEDOT:PSS/**SQ** dyes:$PC_{70}BM$ (1 : 3)/Al device under illumination are shown in Fig. 5 and the PV parameters are compiled in Table 4. The dark *J–V* characteristics of all the devices showed rectification effect indicates the formation of p–n junctions in the BHJ active layer. The device with **TBU-SQ**:$PC_{70}BM$ active layer showed V_{OC} of 0.76 V, J_{SC} of 6.25 mA cm^{-2} and *FF* of 0.36 showed PCE of 1.71%. The device with **EtTBU-SQ**:$PC_{70}BM$ blend showed V_{OC} of 0.66 V, J_{SC} of 6.82 mA cm^{-2} and *FF* of 0.42 showed PCE of 2.15%. Similarly, **MeTBU-SQ**:$PC_{70}BM$ blend showed V_{OC} of 0.68 V, J_{SC} of 7.2 mA cm^{-2} and *FF* of 0.44 showed PCE reaching up to 2.15%. The PCE of the devices based on **MeTBU-SQ** and **EtTBU-SQ** is higher than that for the device based on **TBU-SQ**, which is attributed mainly to the higher value of J_{SC} for these devices. The higher value of J_{SC} is mainly due to the extended absorption band in the near IR region and higher hole mobility. The higher V_{OC} value of the BHJ based on **TBU-SQ** with respect to the other two SQ dyes is attributed to its low-lying HOMO value, since the V_{OC} is directly related to the difference between the HOMO level of donor and LUMO level of acceptor. The IPCE spectra of the devices are also been shown in Fig. 5a for devices based on SQ dyes as electron donor. The IPCE spectra of the devices follow the absorption spectra of the active BHJ employed in the devices. It can be seen from this figure that the IPCE values for **MeTBU-SQ** dye in all wavelength regions is higher than the other two SQ dyes, which is consistent with the higher value of J_{SC} and PCE.

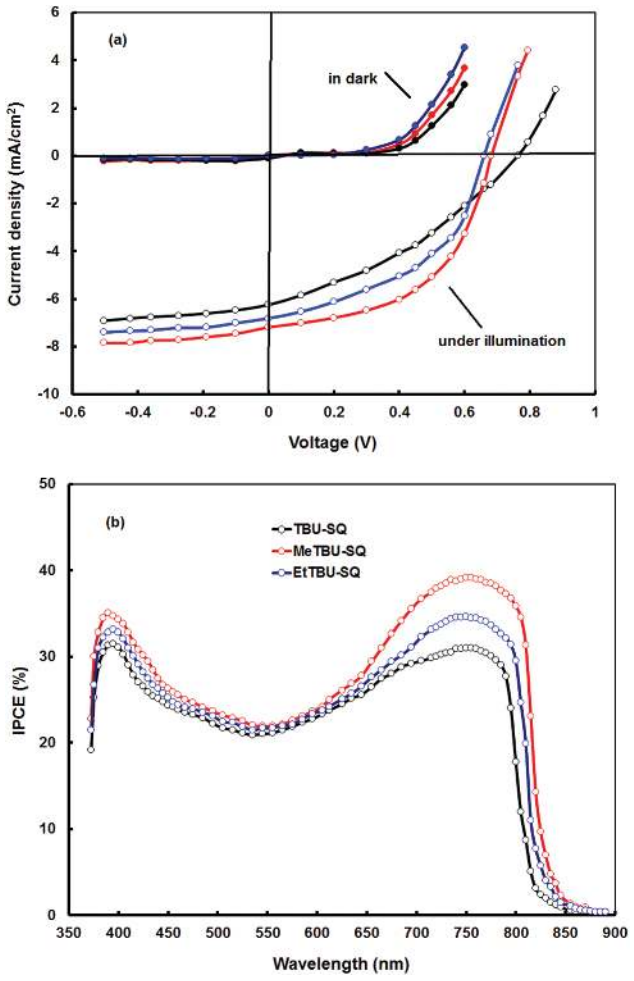

Fig. 5 (a) Current–voltage characteristics in the dark and under illumination, and (b) IPCE spectra for the ITO/PEDOT:PSS/squaraine dyes:$PC_{70}BM$ (1 : 3)/Al devices, where the blend is cast from THF. Black (**TBU-SQ**), red (**MeTBU-SQ**), blue (**EtTBU-SQ**).

Incorporating solvent additives to solutions from which the BHJ layers are cast is widely used for the fabrication of efficient polymer-based devices,[58–63] and has also been successfully applied to other BHJ devices of SM:fullerene derivatives (SM = small molecule).[22,68,69] On the basis of a **MeTBU-SQ**:$PC_{70}BM$ (1 : 3) blend ratio, we examined the role of additive on the PV response of BHJPV devices. Typically, solvent additive concentrations in polymer solutions range between 1 and 5%. We found that using a standard formulation involving DIO and THF leads to a deterioration of device performance relative to a device fabricated from the parent THF solvent. The device fabricated from the blend solutions containing 1% (v/v) DIO showed poor PCE relative to the parent THF solvent. However, decreasing the DIO content leads to an improvement in performance, with the highest efficiency attained for 0.4% (v/v) DIO.

The *J–V* characteristics of the devices in the dark and under illumination, in which **MeTBU-SQ**:$PC_{70}BM$ (DIO–THF) and **MeTBU-SQ**:$PC_{70}BM$ (DIO–THF thermally annealed) blend were used as active layer, are shown in Fig. 6, and PV parameters are compiled in Table 4. It can be seen from the table that the SC processed with 0.4% (v/v) DIO exhibited a significant increase in J_{SC} and *FF* to 8.62 mA cm^{-2} and 0.48, respectively, resulting in PCE of about 2.73%. The PCE of the device was further enhanced up to 3.14% with J_{SC} and *FF* of 9.8 mA cm^{-2} and 0.50, respectively, when the blend film cast from DIO–THF was thermally annealed. The IPCE spectra of the devices based on DIO–THF cast **MeTBU-SQ**:$PC_{70}BM$ blend are shown in Fig. 6b. The higher values of IPCE for these devices are also consistent with the values of J_{SC} and PCE.

In order to have a better charge injection into the acceptor, the donor and the acceptor should interact strongly in the blends. To analyze the interactions in the [SQ···$PC_{70}BM$] complex, we calculated the electrostatic potentials at DFT level, which are shown in Fig. 7. It is found that the negative charge (red color) is localized on the oxygen atoms of the SQ-ring and more positive charge (blue color) is localized on the ester group in $PC_{70}BM$. Thus, among possible interaction configurations of the donor–acceptor complex, the oxygen atom of

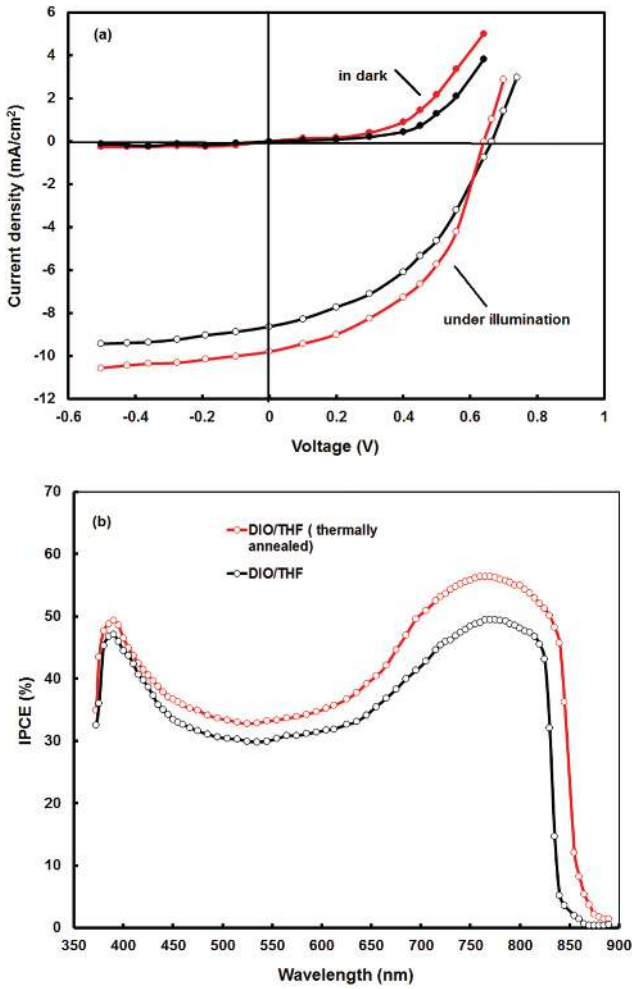

Fig. 6 Current–voltage characteristics in the dark and under illumination, and (b) IPCE spectra for the ITO/PEDOT:PSS/**MeTBU-SQ**:$PC_{70}BM$ (1 : 3)/Al devices, where the blend is cast from DIO–THF. Black for DIO–THF and red for DIO–THF (thermally annealed).

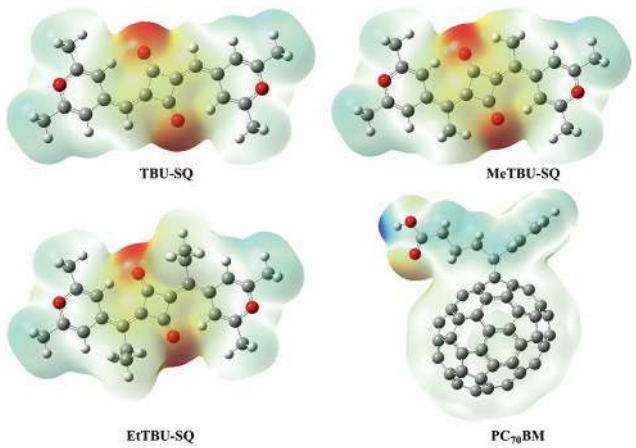

Fig. 7 Electrostatic potentials of all the SQ dyes and $PC_{70}BM$ obtained at B3LYP/6-31G(d,p).

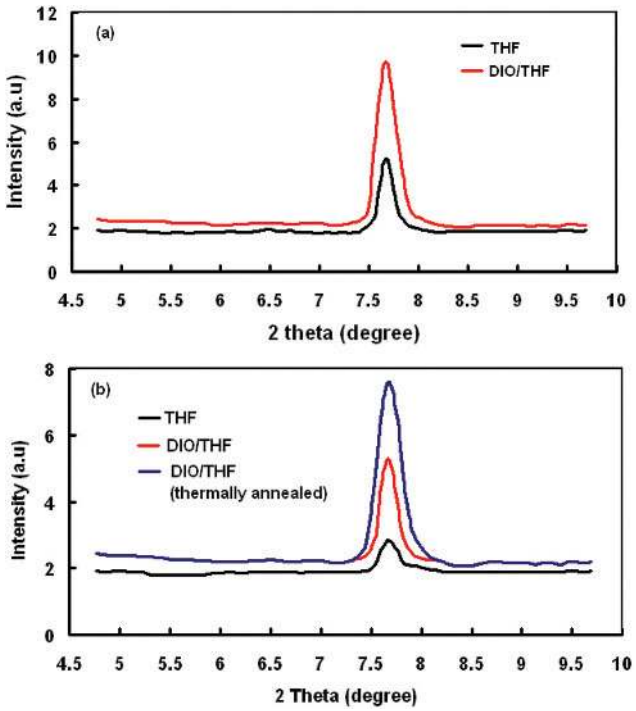

Fig. 8 X-ray diffraction pattern of pristine (a) **MeTBU-SQ** films and (b) **MeTBU-SQ**:$PC_{70}BM$ blend films, cast under different conditions.

$PC_{70}BM$ interacts with the central part of the SQ dyes with a facial orientation for better intermolecular charge transfer.

The X-ray diffraction (XRD) patterns of pure **MeTBU-SQ** thin films (Fig. 8a) show that the peak around 2θ = 7.68° is enhanced when the film is cast from DIO–CF solvent and which is further enhanced after thermal annealing. This indicates that the cast film obtained from mixed solvent could form a more ordered structure as a result of enhanced π–π stacking. The additional application of thermal annealing associated with the film cast from mixed solvent allowed the film to crystallize more extensively, as indicated by the increased absorption intensity and redshift in the absorption band. When **MeTBU-SQ** was blended with $PC_{70}BM$, the diffraction peak around 2θ = 7.68° of the blend cast from CF only becomes weak, suggesting an effective mixing of $PC_{70}BM$ with **MeTBU-SQ** and also suggesting the amorphous nature of the blend film, as shown in Fig. 8b. This indicates that the film cast from CF solvent was not sufficiently crystallized. However, when the same blend was cast from DIO–CF solvent, the diffraction peak at 2θ = 7.68° reappears, which is attributed to the increased crystalline nature of the blend. The intensity of this diffraction peak has been further increased when the blend film cast from DIO–THF solvent is thermally annealed. This also indicates that the thermal annealing further increases the film crystallinity. Therefore, the solvent additive and subsequent thermal annealing leads to an enhancement in the hole mobility. However, the increase in the order of the donor phase probably causes a decrease in the order of the acceptor phase, which leads to the reduction in electron mobility. The

enhancement in the hole mobility and reduction in the electron mobility lead to balanced charge transport, which is beneficial for the better J_{SC} and PCE. The high value of J_{SC} for the cast and thermally annealed blend spin-coated from additive solvent can be attributed to the J-aggregation of the SQ donor, leading to an improved morphology as indicated in the XRD pattern. This arrangement provides better conduction pathways for excitons and holes, while maintaining a sufficiently large interface with acceptor $PC_{70}BM$. Efficient exciton transport in J-aggregates is well documented from natural light harvesting systems based on J-aggregated chlorophylls.[70]

To understand the influence of charge carrier transport on the PV performance, we used the SCLC method to measure the hole and electron mobilities in the blend. Fig. 9 shows the *J–V* characteristics for (a) hole-only and (b) electron-only devices processed and cast from THF, DIO–THF and DIO–THF (thermally annealed). The average hole and electron mobilities for the blends cast from THF were found to be 1.6×10^{-6} and 3.2×10^{-4} cm^2 V^{-1} s^{-1}, respectively. When the blend film was cast from THF–DIO solvent, the hole and electron mobilities estimated from the *J–V* characteristics in the space charge region are 3.5×10^{-5} and 4.1×10^{-4} cm^2 V^{-1} s^{-1}, respectively. Moreover, after annealing the blend cast from DIO–THF solvent, the hole and electron mobilities are increased up to 6.4×10^{-5} and 4.6×10^{-4} cm^2 V^{-1} s^{-1}, respectively. The highly ordered and crystalline nature of the blend used in the BHJSC is known to improve the charge-carrier mobility. Both electron and hole mobility for blend cast from additive solvent is higher than for blend cast from THF solvent, and they are further enhanced upon the thermal annealing. However, the degree of enhancement in hole mobility is higher than that for electron mobility. It has already reported that the ratio of electron and hole mobilities plays an important role in the charge transport and thus for PCE of the SC. For an efficient BHJSC, this ratio should approach unit. This ratio is 200, 12 and 7.2 for BHJ devices processed from THF solvent, DIO–THF solvent and DIO–THF (thermally annealed), respectively. Therefore, the device processed from the additive solvent possesses a more balance transport, which is further improved upon thermal annealing, leading to higher J_{SC}, resulting in enhanced PCE.

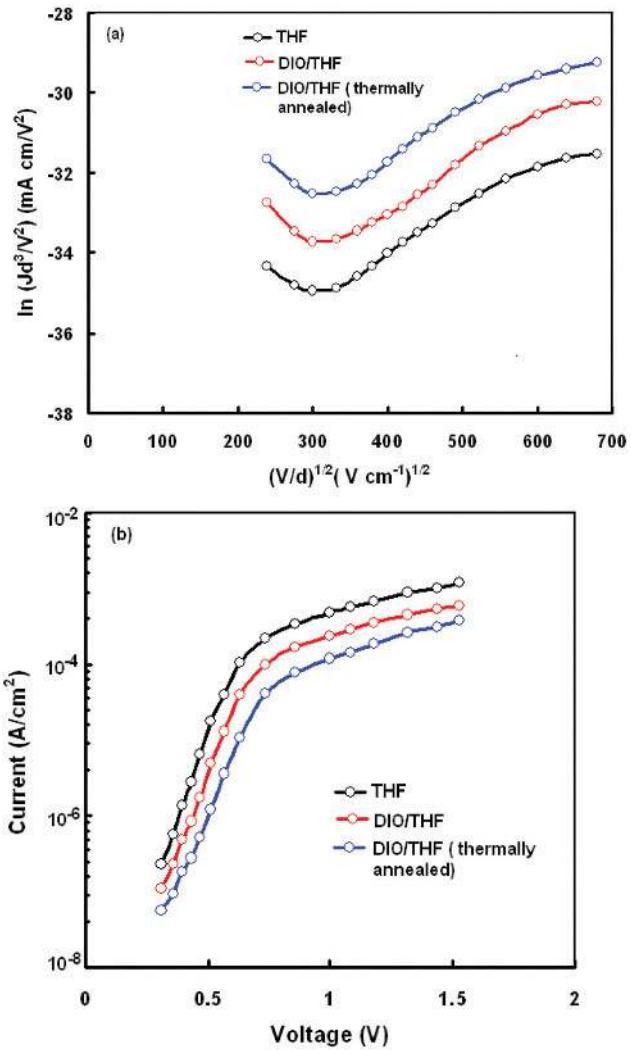

Fig. 9 Current–voltage characteristics in the dark for (a) hole-only and (b) electron-only devices using **MeTBU-SQ**:$PC_{70}BM$ blends.

4. Conclusion

Low bandgap small molecules having SQ chromophores, *i.e.* **TBU-SQ**, **MeTBU-SQ** and **EtTBU-SQ**, have been synthesized and characterized by optical, cyclic voltammetric and XRD measurements and quantum chemical calculations. The optical absorption in the thin film shows a broad absorption band at longer wavelengths and an optical band gap about 1.64–1.75 eV. The electrochemical data, *i.e.* HOMO and LUMO, indicate that these small molecules are well suited for the OBHJSCs. BHJPV devices based on **TBU-SQ**, **MeTBU-SQ** and **EtTBU-SQ** as electron donor and $PC_{70}BM$ as electron acceptor were fabricated from CF. The PCE of the BHJ devices based on **TBU-SQ**:$PC_{70}BM$, **MeTBU-SQ**:$PC_{70}BM$ and **EtTBU-SQ**:$PC_{70}BM$ are 1.71%, 2.15% and 1.89%, respectively, for the blends cast from CF. The higher value of PCE for the **MeTBU-SQ**:$PC_{70}BM$ blend is attributed to the enhanced values of J_{SC} and V_{OC}. The improved crystallinity of **MeTBU-SQ**:$PC_{70}BM$ blend film cast from DIO–THF led to higher PCE (2.73%). The PCE has been further enhanced up to 3.14% for the device based on thermally annealed blend **MeTBU-SQ**:$PC_{70}BM$ cast from DIO–THF solvent. The improved PCE of the BHJPV devices based on **MeTBU-SQ**:$PC_{70}BM$ blend cast from DIO–CF solvent and thermally annealed has been attributed to the improved charge transport in the devices due to the higher hole mobility. All these arguments are supported by the quantum chemical DFT calculations.

Acknowledgements

Financial support from CSIR-TAPSUN project NWP-0054 is acknowledged. BAR, KY and GSK thank CSIR for the

fellowship. We thank the Director, CSIR-IICT for constant support in this work. GDS is sincerely thankful to Prof. Y. K. Vijay, Department of Physics, University of Rajasthan, and Dr S. Biswas, LNMIT, Jaipur, for allowing him to carry out the device fabrication and characterization.

References

1 A. C. Arias, J. D. MacKenzie, I. McCulloch, J. Rivnay and A. Salleo, Materials and applications for large area electronics: solution-based approaches, *Chem. Rev.*, 2010, **110**, 3–24.
2 F. C. Krebs, J. Fyenbo and M. Jorgensen, Product integration of compact roll-to-roll processed polymer solar cell modules: methods and manufacture using flexographic printing, slot-die coating and rotary screen printing, *J. Mater. Chem.*, 2010, **20**, 8994–9001.
3 L.-M. Chen, Z. Hong, G. Li and Y. Yang, Recent progress in polymer solar cells: manipulation of polymer:fullerene morphology and the formation of efficient inverted polymer solar cells, *Adv. Mater.*, 2009, **21**, 1434–1449.
4 Y.-J. Cheng, S.-H. Yang and C.-S. Hsu, Synthesis of conjugated polymers for organic solar cell applications, *Chem. Rev.*, 2009, **109**, 5868–5923.
5 B. Kippelen and J.-L. Bredas, Organic photovoltaics, *Energy Environ. Sci.*, 2009, **2**, 251–261.
6 F. C. Krebs, Fabrication and processing of polymer solar cells: a review of printing and coating techniques, *Sol. Energy Mater. Sol. Cells*, 2009, **93**, 394–412.
7 P.-L. T. Boudreault, A. Najari and M. Leclerc, Processable low-bandgap polymers for photovoltaic applications, *Chem. Mater.*, 2010, **23**, 456–469.
8 C. J. Brabec, S. Gowrisanker, J. J. M. Halls, D. Laird, S. Jia and S. P. Williams, Polymer–fullerene bulk-heterojunction solar cells, *Adv. Mater.*, 2010, **22**, 3839–3856.
9 M. C. Scharber, D. Mühlbacher, M. Koppe, P. Denk, C. Waldauf, A. J. Heeger and C. J. Brabec, Design rules for donors in bulk-heterojunction solar cells—towards 10% energy-conversion efficiency, *Adv. Mater.*, 2006, **18**, 789–794.
10 Y. Li, Molecular design of photovoltaic materials for polymer solar cells: toward suitable electronic energy levels and broad absorption, *Acc. Chem. Res.*, 2012, **45**, 723–733.
11 S. H. Park, A. Roy, S. Beaupre, S. Cho, N. Coates, J. S. Moon, D. Moses, M. Leclerc, K. Lee and A. J. Heeger, Bulk heterojunction solar cells with internal quantum efficiency approaching 100%, *Nat. Photonics*, 2009, **3**, 297–302.
12 H.-Y. Chen, J. Hou, S. Zhang, Y. Liang, G. Yang, Y. Yang, L. Yu, Y. Wu and G. Li, Polymer solar cells with enhanced open-circuit voltage and efficiency, *Nat. Photonics*, 2009, **3**, 649–653.
13 Y. Liang, Z. Xu, J. Xia, S.-T. Tsai, Y. Wu, G. Li, C. Ray and L. Yu, For the bright future—bulk heterojunction polymer solar cells with power conversion efficiency of 7.4%, *Adv. Mater.*, 2010, **22**, E135–E138.
14 C. Piliego, T. W. Holcombe, J. D. Douglas, C. H. Woo, P. M. Beaujuge and J. M. J. Fréchet, Synthetic control of structural order in *N*-alkylthieno[3,4-*c*]pyrrole-4,6-dione-based polymers for efficient solar cells, *J. Am. Chem. Soc.*, 2010, **132**, 7595–7597.
15 T.-Y. Chu, J. Lu, S. Beaupré, Y. Zhang, J.-R. m. Pouliot, S. Wakim, J. Zhou, M. Leclerc, Z. Li, J. Ding and Y. Tao, Bulk heterojunction solar cells using thieno[3,4-*c*]pyrrole-4,6-dione and dithieno[3,2-*b*:2′,3′-*d*]silole copolymer with a power conversion efficiency of 7.3%, *J. Am. Chem. Soc.*, 2011, **133**, 4250–4253.
16 H. Zhou, L. Yang, A. C. Stuart, S. C. Price, S. Liu and W. You, Development of fluorinated benzothiadiazole as a structural unit for a polymer solar cell of 7% efficiency, *Angew. Chem., Int. Ed.*, 2011, **50**, 2995–2998.
17 Y. Liang and L. Yu, A new class of semiconducting polymers for bulk heterojunction solar cells with exceptionally high performance, *Acc. Chem. Res.*, 2010, **43**, 1227–1236.
18 J. Xue, Perspectives on organic photovoltaics, *Polym. Rev.*, 2010, **50**, 411–419.
19 R. F. Service, Outlook brightens for plastic solar cells, *Science*, 2011, **332**, 293.
20 J. Roncali, Molecular bulk heterojunctions: an emerging approach to organic solar cells, *Acc. Chem. Res.*, 2009, **42**, 1719–1730.
21 M. T. Lloyd, J. E. Anthony and G. G. Malliaras, Photovoltaics from soluble small molecules, *Mater. Today*, 2007, **10**, 34–41.
22 B. Walker, C. Kim and T.-Q. Nguyen, Small molecule solution-processed bulk heterojunction solar cells, *Chem. Mater.*, 2010, **23**, 470–482.
23 Z. Li, Q. Dong, Y. Li, B. Xu, M. Deng, J. Pei, J. Zhang, F. Chen, S. Wen, Y. Gao and W. Tian, Design and synthesis of solution processable small molecules towards high photovoltaic performance, *J. Mater. Chem.*, 2011, **21**, 2159–2168.
24 H. Shang, H. Fan, Y. Liu, W. Hu, Y. Li and X. Zhan, A solution-processable star-shaped molecule for high-performance organic solar cells, *Adv. Mater.*, 2011, **23**, 1554–1557.
25 J. E. Anthony, Small-molecule, nonfullerene acceptors for polymer bulk heterojunction organic photovoltaics, *Chem. Mater.*, 2010, **23**, 583–590.
26 B. Walker, A. B. Tamayo, X.-D. Dang, P. Zalar, J. H. Seo, A. Garcia, M. Tantiwiwat and T.-Q. Nguyen, Nanoscale phase separation and high photovoltaic efficiency in solution-processed, small-molecule bulk heterojunction solar cells, *Adv. Funct. Mater.*, 2009, **19**, 3063–3069.
27 G. D. Sharma, P. Suresh, J. A. Mikroyannidis and M. M. Stylianakis, Efficient bulk heterojunction devices based on phenylenevinylene small molecule and perylene–pyrene bisimide, *J. Mater. Chem.*, 2010, **20**, 561–567.
28 J. A. Mikroyannidis, M. M. Stylianakis, P. Balraju, P. Suresh and G. D. Sharma, Novel *p*-phenylenevinylene compounds containing thiophene or anthracene moieties and cyano–

vinylene bonds for photovoltaic applications, *ACS Appl. Mater. Interfaces*, 2009, **1**, 1711–1718.
29 W. Li, C. Du, F. Li, Y. Zhou, M. Fahlman, Z. Bo and F. Zhang, Benzothiadiazole-based linear and star molecules: design, synthesis, and their application in bulk heterojunction organic solar cells, *Chem. Mater.*, 2009, **21**, 5327–5334.
30 J. A. Mikroyannidis, D. V. Tsagkournos, S. S. Sharma, Y. K. Vijay and G. D. Sharma, Low band gap conjugated small molecules containing benzobisthiadiazole and thienothiadiazole central units: synthesis and application for bulk heterojunction solar cells, *J. Mater. Chem.*, 2011, **21**, 4679–4688.
31 Q. Shi, P. Cheng, Y. Li and X. Zhan, A solution processable D–A–D molecule based on thiazolothiazole for high performance organic solar cells, *Adv. Energy Mater.*, 2012, **2**, 63–67.
32 Y. Zhang, X.-D. Dang, C. Kim and T.-Q. Nguyen, Effect of charge recombination on the fill factor of small molecule bulk heterojunction solar cells, *Adv. Energy Mater.*, 2011, **1**, 610–617.
33 Y. Sun, G. C. Welch, W. L. Leong, C. J. Takacs, G. C. Bazan and A. J. Heeger, Solution-processed small-molecule solar cells with 6.7% efficiency, *Nat. Mater.*, 2012, **11**, 44–48.
34 F. Silvestri, M. D. Irwin, L. Beverina, A. Facchetti, G. A. Pagani and T. J. Marks, Efficient squaraine-based solution processable bulk-heterojunction solar cells, *J. Am. Chem. Soc.*, 2008, **130**, 17640–17641.
35 H. Burckstummer, N. M. Kronenberg, M. Gsanger, M. Stolte, K. Meerholz and F. Wurthner, Tailored merocyanine dyes for solution-processed BHJ solar cells, *J. Mater. Chem.*, 2010, **20**, 240–243.
36 G. Wei, S. Wang, K. Renshaw, M. E. Thompson and S. R. Forrest, Solution-processed squaraine bulk heterojunction photovoltaic cells, *ACS Nano*, 2010, **4**, 1927–1934.
37 D. Bagnis, L. Beverina, H. Huang, F. Silvestri, Y. Yao, H. Yan, G. A. Pagani, T. J. Marks and A. Facchetti, Marked alkyl- *vs*. alkenyl-substitutent effects on squaraine dye solid-state structure, carrier mobility, and bulk-heterojunction solar cell efficiency, *J. Am. Chem. Soc.*, 2010, **132**, 4074–4075.
38 S. Wang, E. I. Mayo, M. D. Perez, L. Griffe, G. Wei, P. I. Djurovich, S. R. Forrest and M. E. Thompson, High efficiency organic photovoltaic cells based on a vapor deposited squaraine donor, *Appl. Phys. Lett.*, 2009, **94**, 233304–233303.
39 L. Beverina, M. Drees, A. Facchetti, M. Salamone, R. Ruffo and G. A. Pagani, Bulk heterojunction solar cells – tuning of the HOMO and LUMO energy levels of pyrrolic squaraine dyes, *Eur. J. Org. Chem.*, 2011, 5555–5563.
40 J.-H. Yum, P. Walter, S. Huber, D. Rentsch, T. Geiger, F. Nüesch, F. De Angelis, M. Grätzel and M. K. Nazeeruddin, Efficient far red sensitization of nanocrystalline TiO_2 films by an unsymmetrical squaraine dye, *J. Am. Chem. Soc.*, 2007, **129**, 10320–10321.
41 K. Liang, K.-Y. Law and D. G. Whitten, Estimation of exciton sizes in squaraine monolayers by intralayer photoinduced electron transfer, *J. Phys. Chem.*, 1995, **99**, 16704–16708.
42 A. P. Piechowski, G. R. Bird, D. L. Morel and E. L. Stogryn, Desirable properties of photovoltaic dyes, *J. Phys. Chem.*, 1984, **88**, 934–950.
43 V. Y. Merritt and H. J. Hovel, Organic solar cells of hydroxy squarylium, *Appl. Phys. Lett.*, 1976, **29**, 414–415.
44 S. Paek, H. Choi, C. Kim, N. Cho, S. So, K. Song, M. K. Nazeeruddin and J. Ko, Efficient and stable panchromatic squaraine dyes for dye-sensitized solar cells, *Chem. Commun.*, 2011, **47**, 2874–2876.
45 G. Wei, S. Wang, K. Sun, M. E. Thompson and S. R. Forrest, Solvent-annealed crystalline squaraine:$PC_{70}BM$ (1 : 6) solar cells, *Adv. Energy Mater.*, 2011, **1**, 184–187.
46 A. M. Goodman and A. Rose, Double extraction of uniformly generated electron-hole pairs from insulators with noninjecting contacts, *J. Appl. Phys.*, 1971, **42**, 2823–2830.
47 J.-G. Chen, D.-Y. Huang and Y. Li, Synthesis and properties of near-infrared absorbing asymmetric pyrylium–squarylium dyes containing tertiary butyl groups, *Dyes Pigm.*, 2000, **46**, 93–99.
48 B. He, X. Cai, M. Lu and D. Huang, Synthesis and characterization of novel squarylium dyes, *Dyes Pigm.*, 1999, **41**, 31–34.
49 M. R. Detty and B. Henne, Squarylium dyes based on 2,6-di-*tert*-butylselenopyrylium or telluropyrylium nuclei, *Heterocycles*, 1993, **35**, 1149–1156.
50 M. J. Frisch, G. W. Trucks, H. B. Schlegel, G. E. Scuseria, M. A. Robb, J. R. Cheeseman, J. A. Montgomery Jr., T. Vreven, K. N. Kudin, J. C. Burant, J. M. Millam, S. S. Iyengar, J. Tomasi, V. Barone, B. Mennucci, M. Cossi, G. Scalmani, N. Rega, G. A. Petersson, H. Nakatsuji, M. Hada, M. Ehara, K. Toyota, R. Fukuda, J. Hasegawa, M. Ishida, T. Nakajima, Y. Honda, O. Kitao, H. Nakai, M. Klene, X. Li, J. E. Knox, H. P. Hratchian, J. B. Cross, V. Bakken, C. Adamo, J. Jaramillo, R. Gomperts, R. E. Stratmann, O. Yazyev, A. J. Austin, R. Cammi, C. Pomelli, J. W. Ochterski, P. Y. Ayala, K. Morokuma, G. A. Voth, P. Salvador, J. J. Dannenberg, V. G. Zakrzewski, S. Dapprich, A. D. Daniels, M. C. Strain, O. Farkas, D. K. Malick, A. D. Rabuck, K. Raghavachari, J. B. Foresman, J. V. Ortiz, Q. Cui, A. G. Baboul, S. Clifford, J. Cioslowski, B. B. Stefanov, G. Liu, A. Liashenko, P. Piskorz, I. Komaromi, R. L. Martin, D. J. Fox, T. Keith, M. A. Al-Laham, C. Y. Peng, A. Nanayakkara, M. Challacombe, P. M. W. Gill, B. Johnson, W. Chen, M. W. Wong, C. Gonzalez and J. A. Pople, Gaussian Inc., Wallingford CT, 2009.
51 K. Toyota, M. Ishida, M. Ehara, M. J. Frisch and H. Nakatsuji, Singularity-free analytical energy gradients for the SAC/SAC-CI method: coupled perturbed minimum orbital-deformation (CPMOD) approach, *Chem. Phys. Lett.*, 2003, **367**, 730–736.

52 T. Nakajima and H. Nakatsuji, Second-order perturbative approximation to the SAC/SAC-CI method, *Chem. Phys. Lett.*, 1999, **300**, 1–8.
53 T. Nakajima and H. Nakatsuji, Energy gradient method for the ground, excited, ionized, and electron-attached states calculated by the SAC (symmetry-adapted cluster)/SAC-CI (configuration interaction) method, *Chem. Phys.*, 1999, **242**, 177–193.
54 C. Prabhakar, K. Yesudas, G. Krishna Chaitanya, S. Sitha, K. Bhanuprakash and V. J. Rao, Near-infrared absorption in symmetric squarylium and croconate dyes: a comparative study using symmetry-adapted cluster-configuration interaction methods, *J. Phys. Chem. A*, 2005, **109**, 8604–8616.
55 J. Hou, Z. a. Tan, Y. Yan, Y. He, C. Yang and Y. Li, Synthesis and photovoltaic properties of two-dimensional conjugated polythiophenes with bi(thienylenevinylene) side chains, *J. Am. Chem. Soc.*, 2006, **128**, 4911–4916.
56 Q. Sun, H. Wang, C. Yang and Y. Li, Synthesis and electroluminescence of novel copolymers containing crown ether spacers, *J. Mater. Chem.*, 2003, **13**, 800–806.
57 M. M. Wienk, J. M. Kroon, W. J. H. Verhees, J. Knol, J. C. Hummelen, P. A. van Hal and R. A. J. Janssen, Efficient methano[70]fullerene/MDMO-PPV bulk heterojunction photovoltaic cells, *Angew. Chem., Int. Ed.*, 2003, **42**, 3371–3375.
58 Y. Yao, J. Hou, Z. Xu, G. Li and Y. Yang, Effects of solvent mixtures on the nanoscale phase separation in polymer solar cells, *Adv. Funct. Mater.*, 2008, **18**, 1783–1789.
59 J. Peet, J. Y. Kim, N. E. Coates, W. L. Ma, D. Moses, A. J. Heeger and G. C. Bazan, Efficiency enhancement in low-bandgap polymer solar cells by processing with alkane dithiols, *Nat. Mater.*, 2007, **6**, 497–500.
60 J. S. Moon, C. J. Takacs, S. Cho, R. C. Coffin, H. Kim, G. C. Bazan and A. J. Heeger, Effect of processing additive on the nanomorphology of a bulk heterojunction material, *Nano Lett.*, 2010, **10**, 4005–4008.
61 L. Chang, H. W. A. Lademann, J.-B. Bonekamp, K. Meerholz and A. J. Moulé, Effect of trace solvent on the morphology of P3HT:PCBM bulk heterojunction solar cells, *Adv. Funct. Mater.*, 2011, **21**, 1779–1787.
62 W. Chen, T. Xu, F. He, W. Wang, C. Wang, J. Strzalka, Y. Liu, J. Wen, D. J. Miller, J. Chen, K. Hong, L. Yu and S. B. Darling, Hierarchical nanomorphologies promote exciton dissociation in polymer/fullerene bulk heterojunction solar cells, *Nano Lett.*, 2011, **11**, 3707–3713.
63 G. Ren, E. Ahmed and S. A. Jenekhe, Non-fullerene acceptor-based bulk heterojunction polymer solar cells: engineering the nanomorphology via processing additives, *Adv. Energy Mater.*, 2011, **1**, 946–953.
64 Y. Kim, S. Cook, S. M. Tuladhar, S. A. Choulis, J. Nelson, J. R. Durrant, D. D. C. Bradley, M. Giles, I. McCulloch, C.-S. Ha and M. Ree, A strong regioregularity effect in self-organizing conjugated polymer films and high-efficiency polythiophene:fullerene solar cells, *Nat. Mater.*, 2006, **5**, 197–203.
65 L. Li, G. Lu and X. Yang, Improving performance of polymer photovoltaic devices using an annealing-free approach via construction of ordered aggregates in solution, *J. Mater. Chem.*, 2008, **18**, 1984–1990.
66 Y. D. Park, H. S. Lee, Y. J. Choi, D. Kwak, J. H. Cho, S. Lee and K. Cho, Solubility-induced ordered polythiophene precursors for high-performance organic thin-film transistors, *Adv. Funct. Mater.*, 2009, **19**, 1200–1206.
67 F. Würthner, T. E. Kaiser and C. R. Saha-Möller, J-aggregates: from serendipitous discovery to supramolecular engineering of functional dye materials, *Angew. Chem., Int. Ed.*, 2011, **50**, 3376–3410.
68 A. Tamayo, T. Kent, M. Tantitiwat, M. A. Dante, J. Rogers and T.-Q. Nguyen, Influence of alkyl substituents and thermal annealing on the film morphology and performance of solution processed, diketopyrrolopyrrole-based bulk heterojunction solar cells, *Energy Environ. Sci.*, 2009, **2**, 1180–1186.
69 H. Fan, H. Shang, Y. Li and X. Zhan, Efficiency enhancement in small molecule bulk heterojunction organic solar cells via additive, *Appl. Phys. Lett.*, 2010, **97**, 133302–133303.
70 V. I. Prokhorenko, A. R. Holzwarth, M. G. Müller, K. Schaffner, T. Miyatake and H. Tamiaki, Energy transfer in supramolecular artificial antennae units of synthetic zinc chlorins and co-aggregated energy traps. A time-resolved fluorescence study, *J. Phys. Chem. B*, 2002, **106**, 5761–5768.